Impact of ex-PAN carbon fibers thermal treatment on the mechanical behavior of C/SiC composites and on the fiber/matrix coupling

Clémentine Fellah, James Braun, Cédric Sauder, Fausto G Sirotti, Marie-Hélène Berger

Impact of ex-PAN carbon fibers thermal treatment on the mechanical behavior of C/SiC composites and on the fiber/matrix coupling

C. Fellah , J. Braun , C. Sauder , F. Sirotti , M.-H. Berger

PII: S2667-0569(21)00084-5
DOI: https://doi.org/10.1016/j.cartre.2021.100107
Reference: CARTRE 100107

To appear in: *Carbon Trends*

Received date: 1 June 2021
Revised date: 7 September 2021
Accepted date: 8 September 2021

Please cite this article as: C. Fellah , J. Braun , C. Sauder , F. Sirotti , M.-H. Berger , Impact of ex-PAN carbon fibers thermal treatment on the mechanical behavior of C/SiC composites and on the fiber/matrix coupling, *Carbon Trends* (2021), doi: https://doi.org/10.1016/j.cartre.2021.100107

Impact of ex-PAN carbon fibers thermal treatment on the mechanical behavior of C/SiC composites and on the fiber/matrix coupling

C. Fellah *[a, b], J. Braun [a], C. Sauder [a], F. Sirotti [c, d], M.-H. Berger [b]

[a] Université Paris-Saclay, CEA, Service de Recherches Métallurgiques Appliquées, 91191, Gif-sur-Yvette, France

[b] MINES ParisTech, PSL Research Université, MAT – Centre des matériaux, CNRS UMR 7633, BP 87-1003 Evry, France

[c] Laboratoire de Physique de la Matière Condensée, CNRS, Ecole Polytechnique, IP Paris, 91128 Palaiseau Cedex, France

[d] Synchrotron-SOLEIL & Université Paris–Saclay, Saint-Aubin, Boîte Postale 48, F91192 Gif sur Yvette Cedex, France

* Corresponding author. Clémentine FELLAH, *Laboratoire de Géologie de Lyon : Terre, Planètes, Environnement, Université de Lyon 1, ENS de Lyon, CNRS, UMR 5276, F -69622 Villeurbanne, France*

Tel: +33 4 72 72 84 05. E-mail: clementine.fellah@ens-lyon.fr

Graphical Abstract

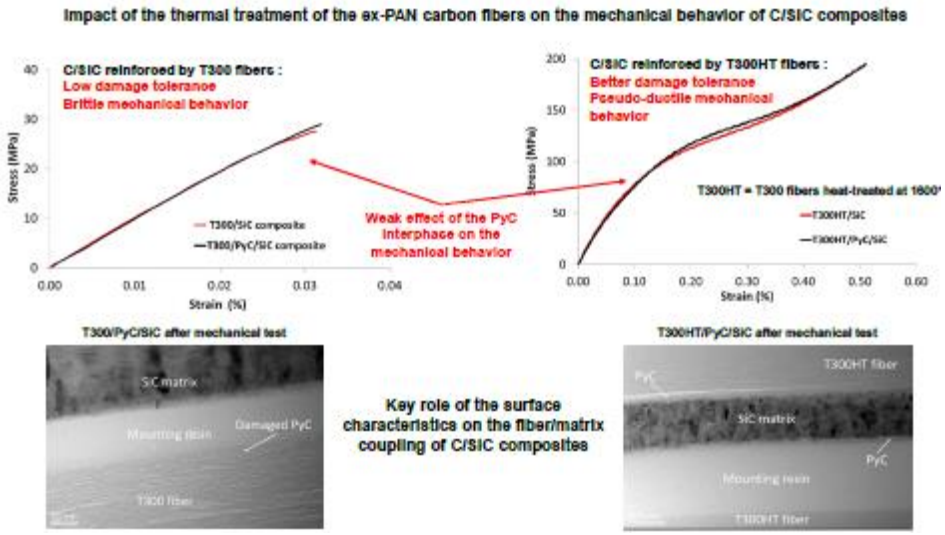

Abstract

Ceramic matrix composites reinforced by external polymerization of acrylonitrile (ex-PAN) carbon fibers with pyrocarbon (PyC) interphase are attractive materials for thermomechanical applications. Nevertheless, C/SiC composites suffer from a low damage tolerance. A 1600°C thermal pretreatment of the carbon fibers led to an improvement of the mechanical properties of the composites. Even if this heat treatment was seen to modify the fiber microstructure and texture, the changes were not sufficient to explain the observed improvements. The consequences of the thermal treatment on carbon fibers were studied by high resolution transmission electron microscopy and physicochemical analyses. The fiber/matrix debonding was also apprehended by analyzing the interfacial regions of C/SiC composites. The key role of the fiber surface structure on the fiber/matrix (F/M) coupling was highlighted. The microstructural reorganization of the heat-treated fibers surfaces induces a high F/M bonding strength and leads to better damage tolerance for the C/SiC composites.

Keywords: Ceramic-matrix composites (CMCs), Interface/Interphase, Microstructural analysis

1. Introduction

The C/SiC composites reinforced by high-strength carbon fibers provide a high mechanical strength at high temperatures (900-1100°C in non-oxidative atmosphere) and have a good resistance to thermal shocks [1]–[3]. Their mechanical properties allow them to be used in aeronautics, aerospace and automotive industries [4]–[6]. However, these materials tend to have a low damage tolerance [7], which reduces their use at high mechanical loads.

The damage tolerance of Ceramic Matrix Composites (CMC) is controlled by the fiber/matrix (F/M) coupling mode [8]. An interphase, such as pyrolytic carbon (PyC), can be deposited between the fiber surfaces and the SiC matrix to tune the fiber/matrix coupling of these materials so as to prevent the matrix cracks to propagate into the fibers by deflecting them at the interface [9], [10]. Matrix micro cracks can be caused by the composite manufacturing process. The cooling down from the Chemical Vapor Infiltration (CVI) process temperature (900°C – 1100°C) generates thermal residual stresses within the composite fibers, interphase and matrix due to differences in thermomechanical properties of each components (Young's modulus, thermal expansion ,…) [11]. These stresses can lead to changes in the F/M coupling and also impact the macroscopic mechanical behavior of the C/SiC composites.

To control the cracks propagation mode, in addition to the PyC interphase, a thermal treatment of the ex-PAN fibers at 1600°C in argon atmosphere, prior the infiltration of the PyC interphase and SiC matrix, was shown to improve the tensile properties of the fibers [12], and consequently those of the C/SiC composite [13]–[15]. This heat treatment induces a modification of the microstructure [16]–[18] and an increase in the fiber stiffness [19], [20]. These modifications of the heat treated ex-PAN fibers provide a pseudo-ductile mechanical

behavior and a better damage tolerance to the C/SiC composites. Nevertheless, it is still difficult to understand the damage mechanisms of heat treated C/SiC composites and the parameters influencing these mechanisms and leading to the improvement of the mechanical behavior of these materials. Therefore, the fibers surface characteristics are one of the parameters to be investigated because they could have been changed after heat treatment. The interfacial interactions in CMC between the interphase and the fiber surface could be influenced by the microstructure and the chemistry of the fiber surfaces [21].

Model C/SiC composites reinforced by T300 fibers, highly common ex-PAN carbon fibers [22], and a PyC interphase were produced for this study. The PyC interphase and the structure and chemistry of the fibers surface roles have been analysed both on the residual stresses development during the composites manufacturing and on the damage tolerance of these materials during mechanical loading. This study has allowed a better understanding of the carbon fibers thermal treatment impact on the mechanical behavior of C/SiC composites and on the fiber/matrix coupling.

2. Experimental procedure

2.1 Materials

The properties of the T300 fibers (Toray Carbon), as given by the manufacturer [23], [24], are listed in Table 1. During the polymer spinning, these ex-PAN carbon fibers undergo a stretching leading to the orientation of the molecular chains along the fiber axis. These fibers are bundled and made infusible by crosslinking at 200-300°C in air and under electric tension in order to maintain the molecular orientation. They are then carbonized in nitrogen between 1000 and 1500°C [25]. The turbostratic structure of this carbon fiber is composed of a random arrangement of graphene sheets (Csp^2), cross-linked to each other [26]–[28]. The T300 fibers

are coated with a polyepoxide resin sizing to protect them during the textile forming processes.

Properties	T300 fiber
Yarn type	FT300B-3000-50B
Yield (g/km)	199
Density (g/cm^3)	1.76
Sizing amount (%w.)	1.1
Ultimate tensile strength (MPa)	3813
Tensile modulus (GPa)	231
Ultimate tensile strain (%)	1.65

Table 1. Properties of T300 fibers.

Interlock 2.5D woven fabrics with 0° and 90° fiber orientations were produced. The sizing was removed after the weaving by thermal treatment at temperature between 900°C and 1100°C. Some of the fabrics were then treated up to 1600°C for two hours after a heating rate of 900°C/h in argon atmosphere. These fibers are named T300HT fibers to differentiate them from only desized T300 fibers.

Then, the fiber fabrics, made of T300 or T300HT fibers were processed by CVI to deposit at first a pyrocarbon interphase (PyC) from C_3H_8, then a SiC matrix from MTS + H_2 at temperatures under 1100°C or only the SiC matrix (Figures 1a. – 1d.). The carbon precursor gases were stopped a few minutes before introducing the SiC precursor gases. The fiber volume fraction within these composites reached 30 - 40 %. The deposited pyrocarbon was highly anisotropic and was ~ 50 nm thick to optimize the fiber/matrix coupling [29].

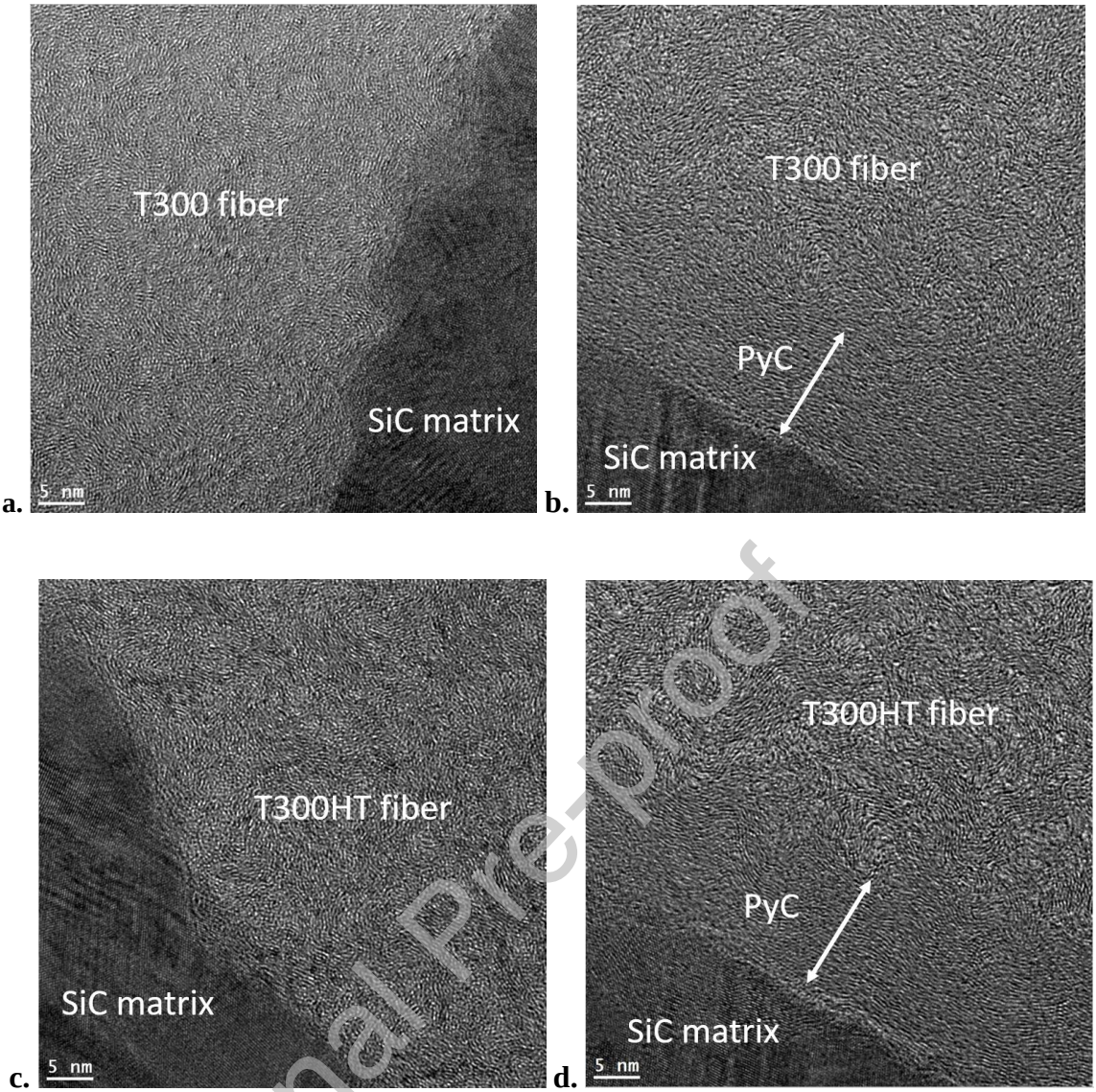

Figure 1. TEM cross-section of the interface of T300/SiC (a.), T300/PyC/SiC (b.), T300HT/SiC (c.) and T300HT/PyC/SiC (d.) composites**.**

The final C/SiC composites presented a porosity between 11 and 13.5 %. The porosity was measured by optical microscopy of polished sections taken in the composites samples and after processing of the images obtained by the Areas de MICROVISION Instrument^{TM} software (Figure 2).

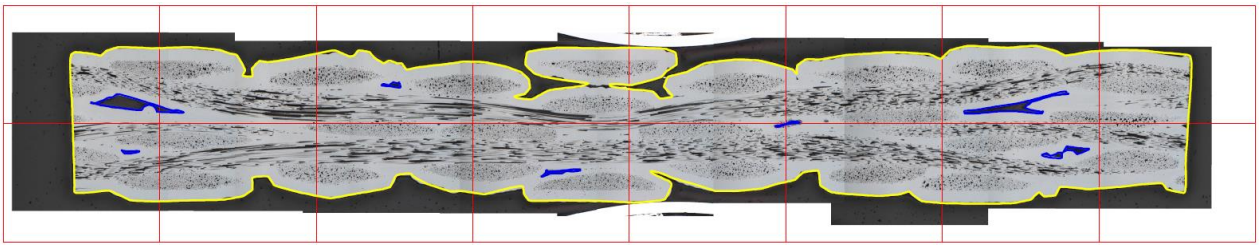

Figure 2. Polished section of a composite processed by the MICROVISION Instrument™ Areas software. The section is delimited in yellow and the porosities are indicated in blue.

2.2 Chemical analysis

High Resolution X-Ray Photoemission Spectroscopy (HRXPS) was chosen to study the chemistry and bonding configuration of T300 and T300HT fibers surface. These analyses were performed on the TEMPO beamline (Time resolved Experiments on Materials with Photoelectron Spectroscopy) of SOLEIL synchrotron (Paris-Saclay, France) [30]. The synchrotron beam had a diameter of 100 µm and its energy was tuned at 700 (baseline energy for the experiment) and 1000 eV to probe any changes in chemistry in the near surface region from 2 to 6 nm below the surface. This probing depth is considered to be three times the inelastic mean free path of the photoelectrons [31]. High-resolution spectra of carbon core level (C_{1s} peak) were recorded and fitted using XPS CASA software. The XPS line shape was represented by a symmetrical Gaussian-Lorentzian function. The Csp^2 component was fitted by an asymmetrical model (Doniach-Sunjic function). A Shirley background subtraction was applied for the high-resolution spectra.

2.3 Mechanical tests

Several studies have shown that the cooling at the end of the CVI process of C/SiC composites leads to a high crack density [11], [32]–[34]. Differences between the fiber,

interphase and matrix coefficients of thermal expansion (CTE) and thermomechanical properties generate residual stresses. Longitudinal, radial and circumferential thermal residual stresses were estimated using an analytical method on a micro-composite model as described by A. Michaux [35], derived from Z. Haskin's model [36], [37]. The C/SiC micro-composite was supposed to be symmetrical along its axis and infinite in its length. The temperature field in the composite was considered uniform, the interfacial bonds were perfect and the mechanical behavior of the components was elastic. The model includes the thermomechanical characteristics of each component: longitudinal and transversal moduli (E_l and E_t), Poisson's ratio (ν), longitudinal and transversal CTE (α_l and α_t). A polynomial equation was used to describe these characteristics as a function of the temperature [35] :

$$Y = A.T^3 + B.T^2 + C.T + D$$

Where A, B, C and D are constants, T the temperature (°C) between 25 and 1000 °C (representative of the CVI infiltration temperature) and Y the thermomechanical characteristics. The following table (Table 2) summarizes the set of the coefficients used for this computation.

	CVI SiC Matrix	**PyC**	**T300 Fiber**	**T300HT Fiber**
E_l (MPa)	$A = -9.85.10^{-5}$ $B = 0.136$ $C = -71.1$ $D = 418.10^3$	$D = 115.10^3$	$D = 230.10^3$	$D = 250.10^3$
E_t (MPa)	$= E_l$	$D = 30.10^3$	$D = 23.10^3$	$D = 25.10^3$
ν	$D = 0.2$	$D = 0.3$	$D = 0.3$	$D = 0.3$
α_l (°C^{-1})	$B = -4.51.10^{-12}$ $C = 9.36.10^{-9}$ $D = 1.30.10^{-6}$	$B = -3.25.10^{-12}$ $C = 5.71.10^{-9}$ $D = 0.765.10^{-6}$	$A = -5.16.10^{-16}$ $B = -9.84.10^{-13}$ $C = 4.04.10^{-9}$ $D = -4.05.10^{-7}$	$A = 1.19.10^{-15}$ $B = -4.17.10^{-12}$ $C = 5.68.10^{-9}$ $D = -8.58.10^{-7}$

α_t (°C^{-1})	= α_l	C = 2.00.10^{-9} D = 10.10^{-6}	B = 4.77.10^{-24} C = -3,26.10^{-10} D = 5,76.10^{-6}	B = -6.03.10^{-13} C = -1.17.10^{-9} D = 7.65.10^{-7}

Table 2. Coefficients used in analytical model for thermally induced residual stresses computation [12], [38], [39].

An Instron 2404 tensile testing machine was used for tensile tests on C/SiC composites. Tensile specimens were 55 mm in length, 8 mm in width and 1.5 mm thick [39], [40]. The gauge length was 25 mm. Uniaxial tensile tests (using a 25 kN load cell) were performed along the 0° fiber orientations at room temperature. The crosshead displacement rate was 0.05 mm/min to 0.2 mm/min and specimen elongation was measured with an extensometer fixed onto the plates (Instron 2620-603). The displacement speed was raised during loading-unloading tensile tests to limit the duration of tests. There was no influence of displacement rate in this range (0.05 to 0.2mm/min). The fracture surfaces were examined by scanning electron microscopy (SEM FEI Nova NanoSEM 450).

2.4 Microstructural analysis

The structural organization of the interfaces of C / (PyC) / SiC composites was investigated by high-resolution transmission electron microscopy (HRTEM). A FEI Tecnai F20 ST operating at 200 kV was employed to record carbon (002) lattice fringe images of the composite interface regions before and after mechanical loading. Thin foils of the surface of T300 and T300HT fibers were prepared by Focused Ion Beam (MEB-FIB Zeiss Auriga 40) and those of C/SiC and C/PyC/SiC composites by Ion Slicer (Jeol IS). Regions near the crack propagation after tensile tests were also extracted by FIB following the lift-out method.

3. Results

3.1 Characterization of carbon fibers surface

The carbon fibers surface chemistry after desizing (T300) and after thermal treatment at 1600°C (T300HT) was analyzed by XPS at 700 eV and 1000 eV (Table 3). Photoemission spectra obtained at 700 eV are shown in Figure 3. All fibers surfaces are carbon-rich (> 90 % at.) with a C_{1s} peak at 285 eV and oxygen, nitrogen, silicon and calcium were also detected (from O_{1s}, N_{1s}, Si_{2p} and Ca_{2p} peaks at 530, 410, 103 and 350 eV respectively). The peak around 190 eV binding energy corresponds to the Oxygen Auger transitions and the one around 437 eV to the Carbon Auger transitions. The photoelectrons kinetic energy axis was introduced in the top of the Figure 2 to immediately identify C-N-O Auger lines. The peak at 25 eV binding energy comes from the superposition of s and p lower shell photoemission of Ca, O and N. The nitrogen content was reduced for T300HT fibers surface in comparison with T300 fibers surface (resp. 2.0 % at. for T300 fibers and 0.9 % at. for T300HT fibers at 700 eV) [41]–[43]. Moreover, nitrogen and oxygen concentration increase along with the probed depth (higher incident energy) for the T300 fibers but remain constant for the T300HT fibers. The calcium detected may originated from the aqueous bath in which the sizing was added. The silicon, rarely mentioned in the composition of carbon fibers, could result from a pollution during the desizing or heat treatment in the CVI chamber previously exposed to SiC deposition, or come from the fibers sizing [44].

Energy	Fibers	C_{1s} (% at.)	O_{1s} (% at.)	N_{1s} (% at.)
700 eV	T300	96.3	1.7	2.0
	T300HT	97.2	1.9	0.9
1000 eV	T300	93.9	2.1	4.0
	T300HT	96.9	2.1	1.0

Table 3. Chemical composition of the T300 and T300HT fibers surface as a function of the incident energy.

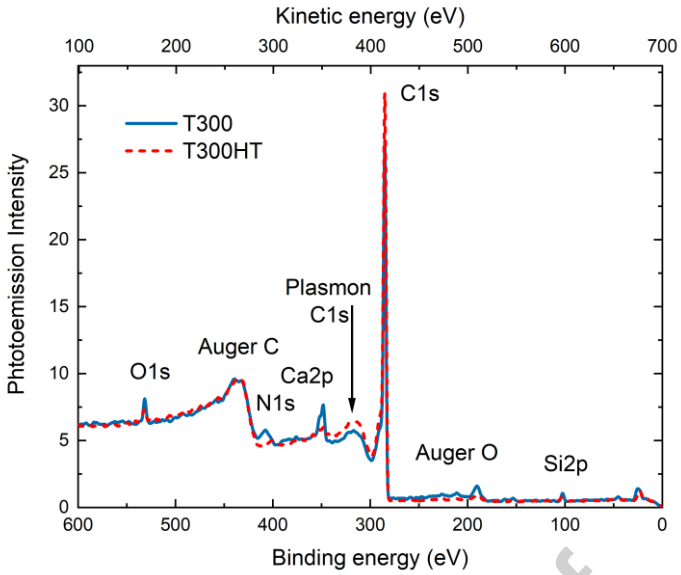

Figure 3. Overview spectra of the T300 and T300HT fibers surfaces at 700 eV.

The C_{1s} peak deconvolution at 700 eV revealed different contributions of carbon bonds (Csp^2, Csp^3, C-O, C-O-C, C-N, C-O, C=O, COOR and COOH) [45]–[51] for both fibers as shown in Figures 4a. and 4b. The sp^2 hybridized C-C was the major carbon bonding mode in T300 and T300HT fiber surfaces. The C-N bonds were more prevalent for T300 fibers surface. Carbon-oxygen bonds were also observed, and were attributed to pollution of the fiber extreme surface. This contamination carbon, named "adventious carbon" by T. L. Barr and S. Seal [52], could deposit on the fibers surface when exposed to air through hydrocarbons containing many C-O-C and C-O bonds. Moreover, the ratio of C=O, COOR and COOH functional groups was significantly higher at the T300HT fibers surface. The proportion of C=O, COOR and COOH bonds, which significantly promote fiber surface reactivity and fiber/matrix bonds within composites [53], is higher on the surface of T300HT fibers and can be partially attributed to plasmonic excitations present in a graphite phase [54].

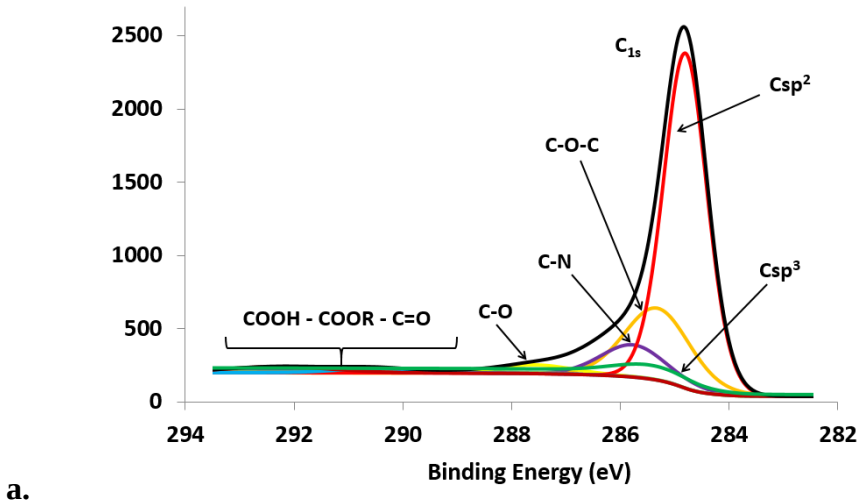

a.

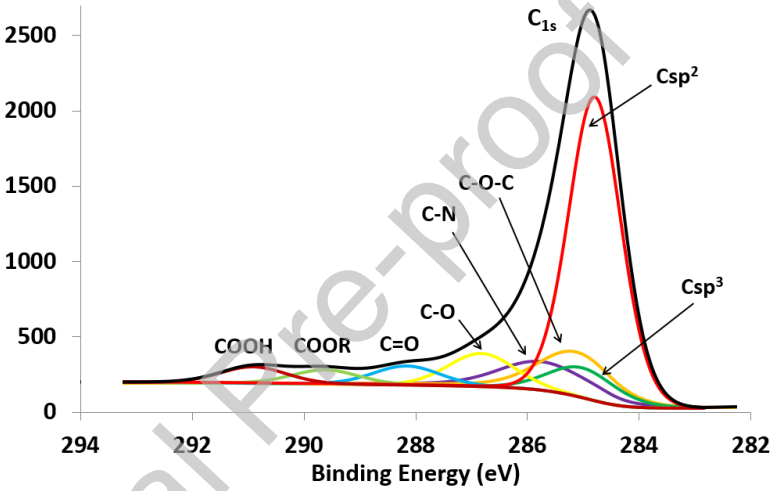

b.

Figure 4. High-resolution spectra of carbon (C_{1s} peak) on the surface of the desized T300 (a.) and T300HT (b.) fibers at 700 eV.

The HRTEM in Figures 5a. and 5b. show the carbon restructuration after the 1600°C heat treatment. The decrease in the inter-reticular distance of T300HT fibers and the formation of nanopores are observed. The value of this distance is 0.36 nm for T300 fibers and 0.352 nm for T300HT fibers. This reorganization is correlated with the nitrogen loss at the edges of isolated USBs (basic structural unit) described by M. Guigon [18], leading to the stacking of the graphene sheets and their lateral connections. The carbon plans on the T300HT fibers surface are more organized than the T300 fibers one, based on the Fast Fourier Transform

(FFT) obtained from HRTEM images. The diffraction rings in the FFT of T300HT fiber are more oriented and thinner.

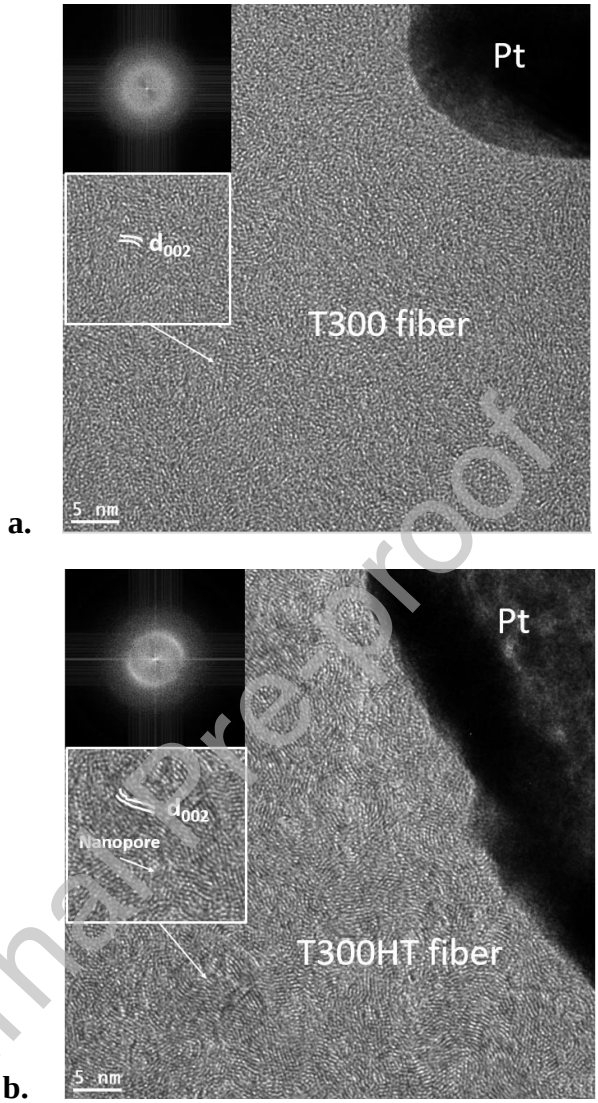

Figure 5. HRTEM images and FFT (top left) of the surface of T300 fiber (i.e. without heat treatment) (a.) and T300HT fiber (after 1600°C heat treatment) (b.). The platinum layer (Pt) was applied for the preparation of these samples by FIB.

3.2 F/M coupling of C/SiC and C/PyC/SiC composites

The strength of the fiber/matrix coupling in the four studied composites were investigated. The thermal residual stresses were estimated using the model presented in section 2.3 and the

phase cohesions in the interfacial regions prior to any external loading were characterized using TEM.

3.2.1 Thermal residual stresses distribution

The axial, radial and hoop residual stresses estimated in the different components of the T300/SiC and T300/PyC/SiC microcomposites are presented Figures 6a. and 6b. [35], [55]. The fiber and the matrix are subjected to strong residual thermal axial stresses, respectively in compression (-550 MPa) and tension (above 300 MPa) in C/SiC composites. In comparison, the radial and the hoop stresses are very low with values below 20 MPa. As expected, given the thickness of the PyC interphase (50 nm), no change in the stresses values were noticed for T300/PyC/SiC microcomposites. The residual radial and hoop stresses at the interphase of T300/PyC/SiC composite are also very low.

The thermal residual stresses were also investigated in the T300HT-reinforced composites to evaluate any changes coming from the fibers thermal treatment (Figures 6c. and 6d.). The residual stresses, especially the axial ones (above 550 MPa compression in the fiber), are slightly higher in the composite reinforced by T300HT fibers than the one reinforced by T300 fibers due to the T300HT fiber microstructural reorganization of the carbon planes in the direction of the fiber axis. This reorganization increased both the fiber stiffness and the CTE, and amplified the differences with the SiC ones resulting in higher residual stresses in T300HT-based composites. Once again, the residual stresses did not change significantly with the presence of a PyC interphase.

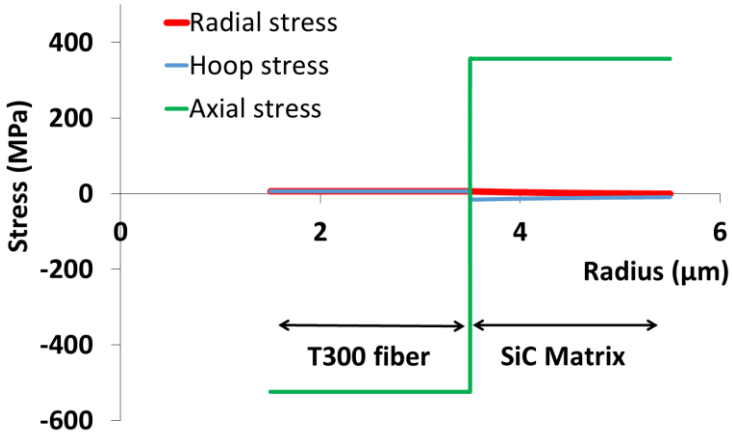

a.

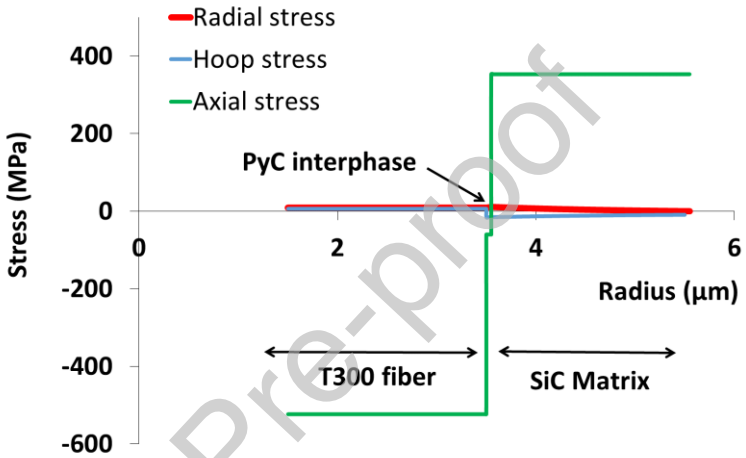

b.

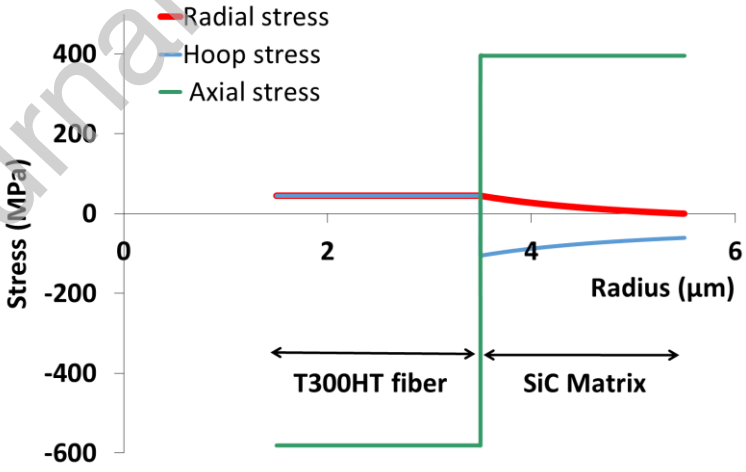

c.

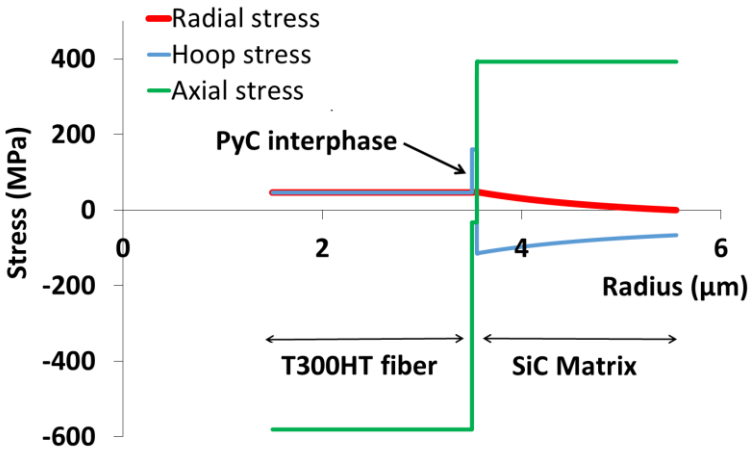

d.

Figure 6. Distribution of the radial, hoop and axial residual stresses for T300/SiC (a.), T300/PyC/SiC (b.), T300HT/SiC (c.) and T300HT/PyC/SiC (d.) composites. The red curve of the radial stress is below the blue hoop stress one.

3.2.2 Interfacial microstructural analysis

TEM and HRTEM observations were conducted on the 2.5D composites prior loading. Some local interfacial debondings between T300 fibers and SiC matrix for T300/SiC composite were revealed (Figures 7a. and 7b.). The mounting resin is embedded in these interfacial debondings regions during the sample preparation. The strong axial residual stresses within the SiC matrix of these C/SiC composites (> 300 MPa) exceeding the failure stress of the CVI SiC matrix, matrix cracks were generated on cooling. In the T300/SiC composite, the matrix cracks reaching the fiber resulted in fiber/matrix decohesions.

In the T300/PyC/SiC composite, a decohesion of the PyC interface was observed, one side attached to the fiber (Figure 7c.) the other to the matrix (Figure 7d.). This highlights the strong interfacial bonds between the fiber and the PyC as well as between the PyC and the matrix. These observations indicate that the integrity of PyC interphase was compromised prior to external loading, during composites processing cool-down step.

The matrix cracks propagation also resulted in local interfacial debonding between T300HT fibers and SiC matrix for T300HT/SiC manufacturing composite. However, some discrepancies regarding the damage mechanisms on interfacial regions were observed. A weakly organized phase, with density variations, was detected within the interfacial debonded region (Figure 7e.). The bonds between the graphene layers of the T300HT fiber surface and the SiC matrix broke heterogeneously. A clear decohesion was not obtained in these regions, on the contrary to what was observed in T300/SiC composite. Furthermore, thin carbon layers attached to the SiC matrix indicates the debonding could have occured in the first ten nanometers below the T300HT fiber surface (Figure 7f.). The carbon-rich regions derived from the fiber are distinguished by EDX from the embedding resin by a lower oxygen and nitrogen content.

For the T300HT/PyC/SiC composite, the debonding was observed at the T300HT/PyC interface although the precise location of the fiber/PyC interface on the HRTEM cross-section in Figure 7g. is not clear. The damage mechanisms were similar to those observed for T300HT/SiC composite. A weakly organized phase with density variations was also observed in the T300HT/PyC interfacial region denoting its partial debonding (Figure 7h.). The PyC interface remained bonded to the SiC matrix, indicating that the PyC/SiC interface was stronger than the T300HT/PyC one.

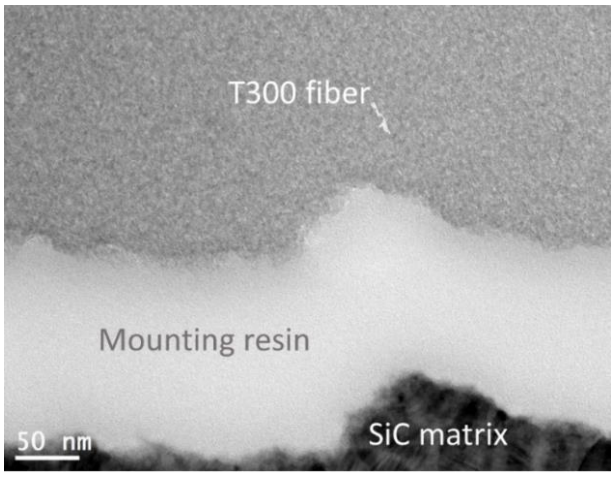

a.

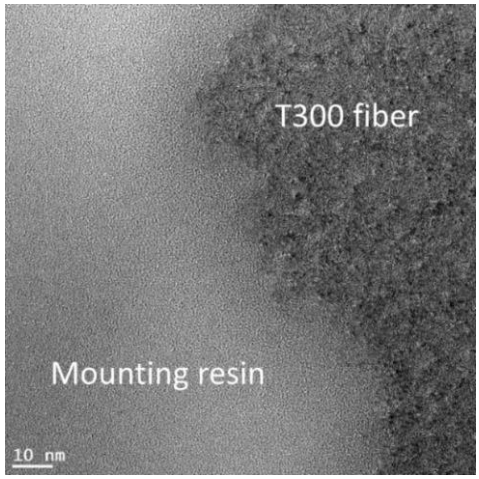

b.

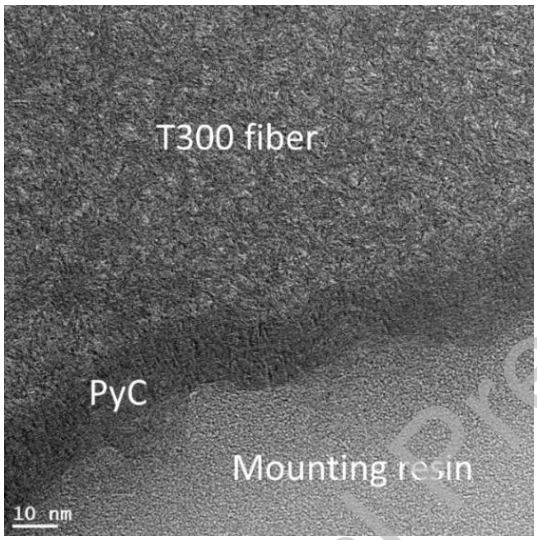

c.

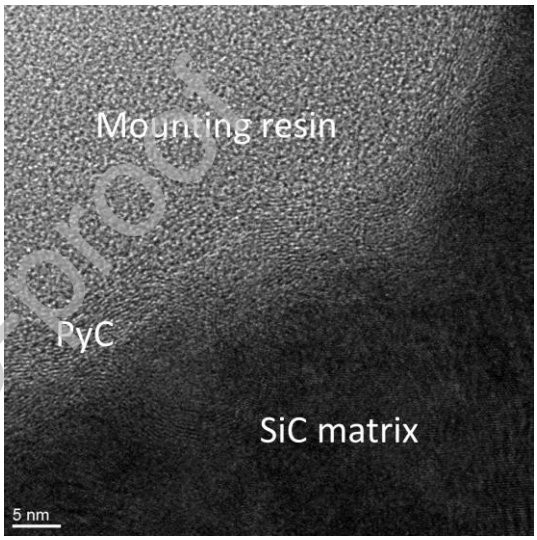

d.

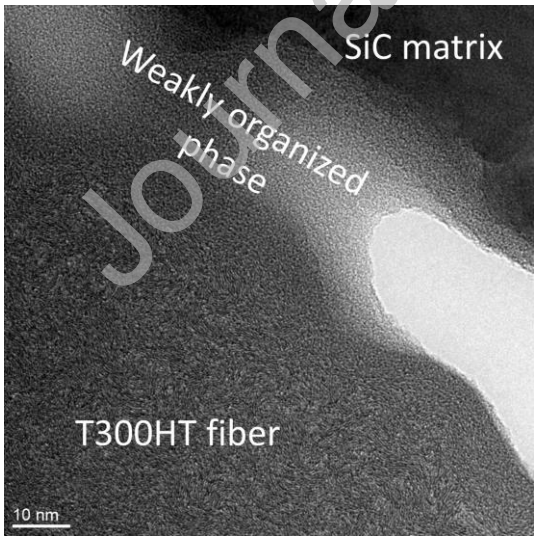

e.

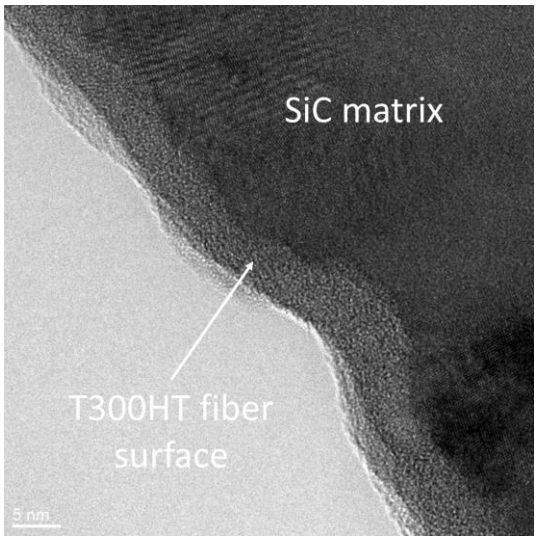

f.

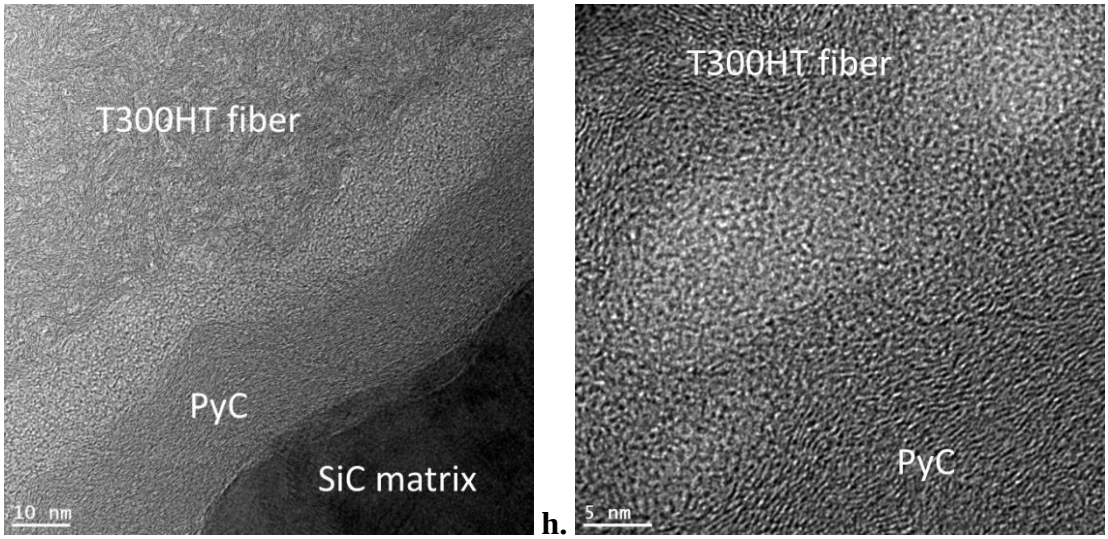

g. **h.**

Figure 7. HRTEM cross-section of the F/M debonding prior to external loading of T300/SiC (a. and b.), T300/PyC/SiC (c and d), T300HT/SiC (e and f) and T300HT/PyC/SiC (g and h) composites at different scales.

3.3 Mechanical behavior of C/SiC and C/PyC/SiC composites

3.3.1 Tensile tests

The room temperature tensile properties of the C/SiC and C/PyC/SiC composites reinforced by T300 or T300HT fibers are presented in Table 4. The stress-strain curves of these composites at room temperature are shown in Figure 8.

The T300/SiC and T300/PyC/SiC composites exhibited a nonlinear elastic domain and brittle mechanical behavior . On the contrary to what was expected, the PyC interface did not increase the damage tolerance of the T300/PyC/SiC compared to the T300/SiC one: the failure strain (ε_r ~ 0.03%) and failure stress (σ_r ~ 28 MPa) of the two composites were equivalent. When the composites were reinforced by T300HT fibers, the mechanical behavior was significantly improved, with a tolerance to mechanical strain and stress that increased by one order of magnitude (ε_r ~ 0.5 % and σ_r ~ 190 MPa). Once again the failure characteristics of the T300HT/SiC and T300HT/PyC/SiC composites were equivalent. These result firstly

show that the PyC interphase does not play a major role on the fracture modes of the composite, since the two composites have similar mechanical behaviors, and secondly that the heat treatment of the carbon fibers has a beneficial effect on the strength and damage tolerance of the composites [12].

	E (GPa)	σ_r (MPa)	ε_r (%)
T300/SiC	103	28	0.03
T300HT/SiC	102	193	0.50
T300/PyC/SiC	98	29	0.03
T300HT/PyC/SiC	94	193	0.51

Table 4. Main mechanical properties of T300 and T300HT reinforced composites: E, σ_r and ε_r.

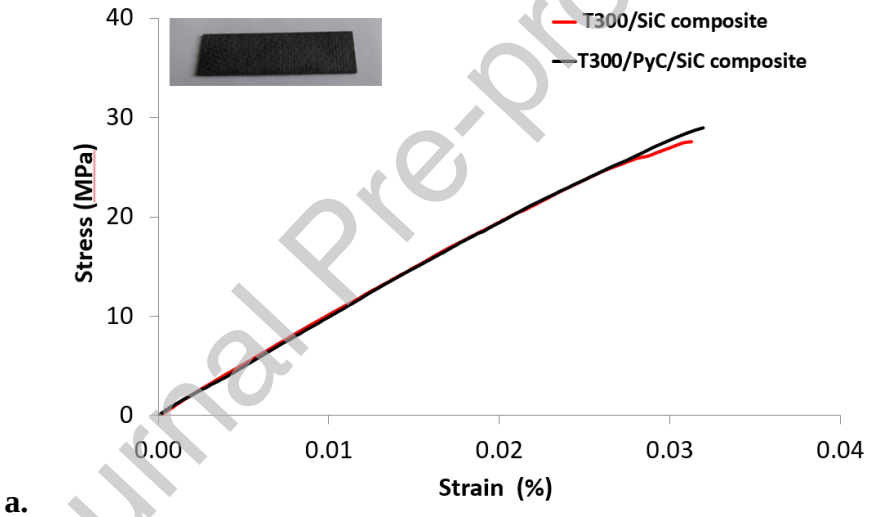

a.

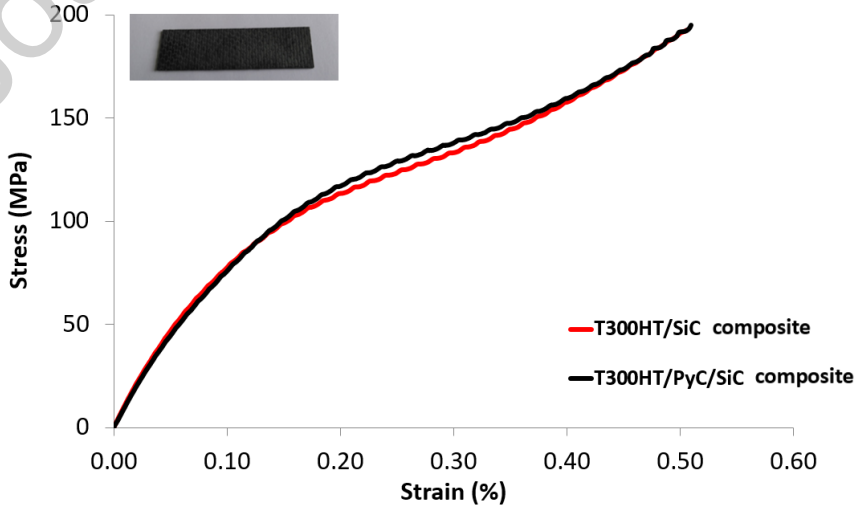

b.

Figure 8. Tensile stress-strain curves for C/SiC and C/PyC/SiC composites reinforced by T300 (a.) and T300HT (b.) fibers with and without a PyC interphase.

It must be noticed that the four composites have similar Young's moduli, lower than those of T300 fibers (~ 230 MPa) and SiC matrix (~ 410 MPa) and that the stiffness increase of the T300HT is not translated to the composite. This is explained by the thermal residual stresses that have generated multi-cracking and fiber/matrix decohesions before tensile loading in the 2.5 D composites.

3.3.2 Fracture morphologies

As expected, due to fragile mechanical behavior, no fiber pull-outs were observed on the fracture surfaces in the T300-reinforced composites (Figure 9a.). Failure surfaces are flat, matrix cracks propagated without being deflected around the fibers even in the presence of PyC, which thereby did not play its role of crack deflector (Figures 9b., 9c. and 9d.).

a.

b.

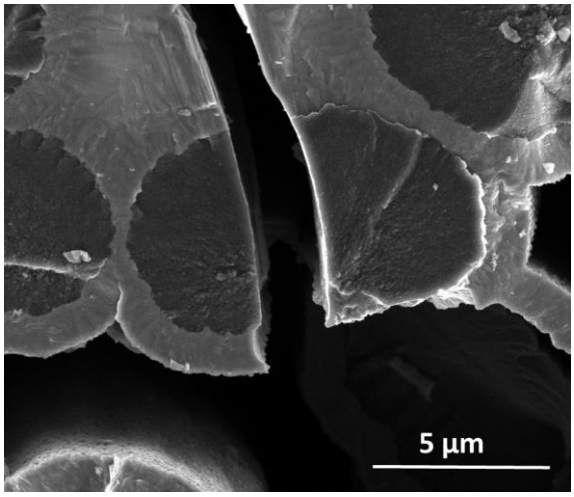

c.

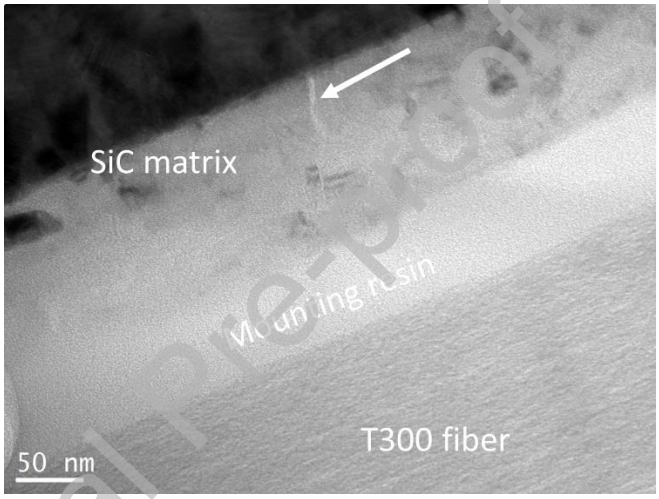

d.

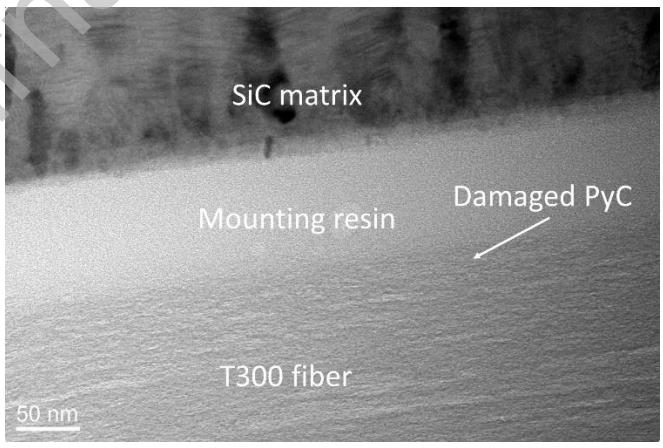

Figure 9. Fracture surface of T300/PyC/SiC composite by SEM (a. and b.) and TEM cross-section of the F/M interface of T300~~H~~/SiC (c.) and T300/PyC/SiC (d.) composites after tensile tests.

On the contrary, T300HT fiber pull-outs were observed for both T300HT/SiC and T300HT/PyC/SiC composites (Figure 10a.). In the T300HT/SiC composite, the heterogeneous debonding that was noticed prior to loading was no more observed in the thin foil extracted just below the failure surfaces, where the fiber and SiC matrix were entirely debonded (Figure 10b.). For the T300HT/PyC/SiC composite, the debonding occurred between the pyrocarbon interphase and the fibers surface, where a weakly organized carbon phase with density variations was noticed prior to the loading (Figure 10c.). The matrix cracks deflection took place within this interfacial damaged region. It was difficult to determine, even using HRTEM, the exact location of the crack path with respect to the two carbon phases, the PyC, the T300HT fiber, or their interface.

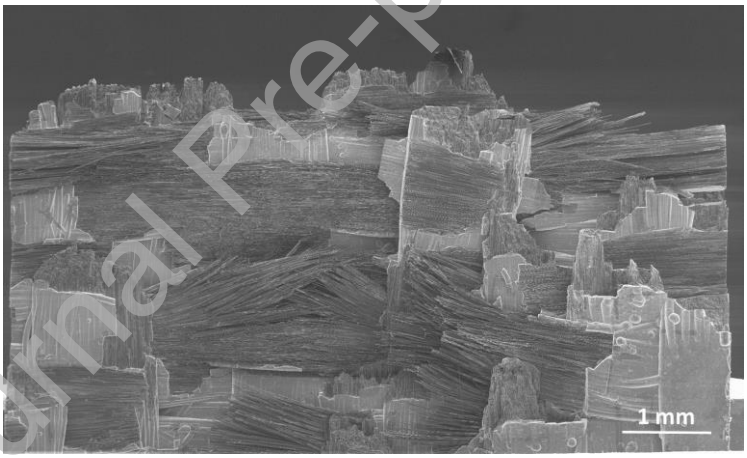

a.

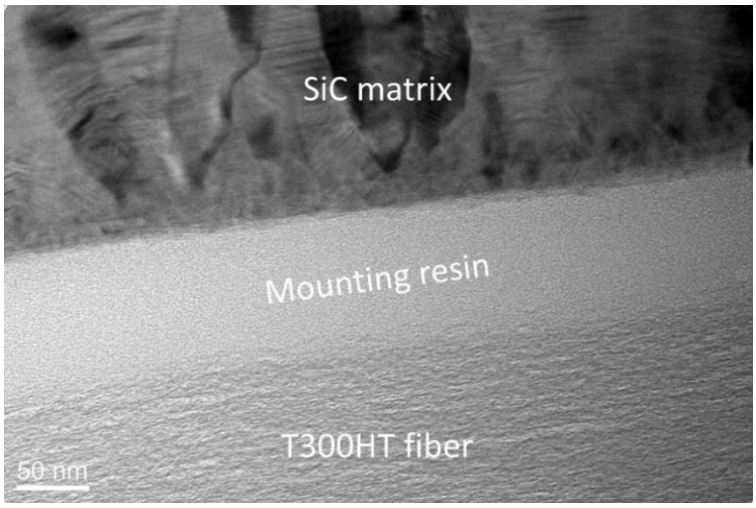

b.

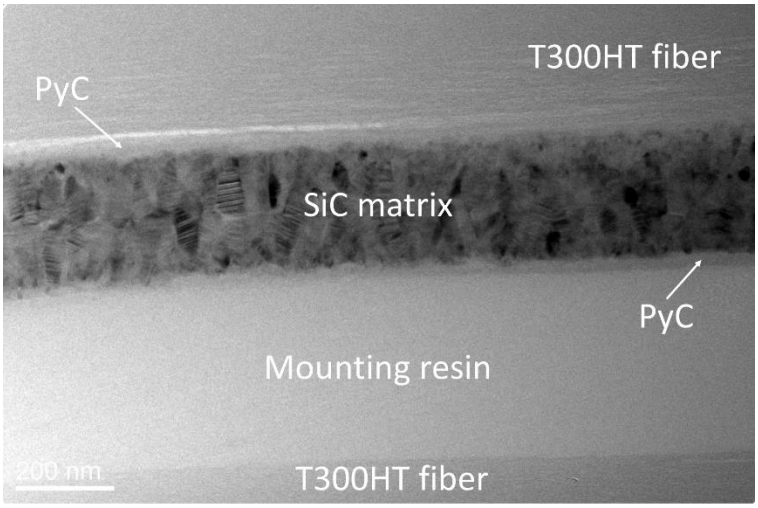

c.

Figure 10. Fracture surface of T300THT/PyC/SiC composite by SEM (a.) and TEM cross-section of the F/M interface of T300HT/SiC (b.) and T300HT/PyC/SiC (c.) composites after tensile tests

4. Discussion

The characterization of the T300 fibers by high-resolution photoemission spectroscopy and TEM showed that the microstructural organization and the chemistry of the fibers surface change after a heat treatment at 1600°C for 2h in argon. During this treatment, the decrease in the C-N bonds fraction in T300 fibers leads to a growth of coherent domains resulting in a higher microstructural organization and anisotropy of the carbon fiber. In addition, the higher ratio of carbon-oxygen bonds on the T300HT fibers surface, C=O, COOH and C-O, could improve its surface reactivity. These surface characteristics have an impact on the organization and the microstructural parameters of the first pyrocarbon planes deposited on the fibers during the manufacture of C/PyC/SiC composites.

The high residual thermal stresses, particularly in the axial direction, explain the SiC matrix cracking occuring during the cooling of the composites. These residual stresses are equivalent in the T300/SiC and the T300HT/SiC composites. Nevertheless, regardless to the presence of

PyC, T300/SiC composites exhibit a brittle behavior without fiber pull-out, whereas T300HT/SiC develop a higher damage tolerance with fiber debonding.

A strong cohesion is promoted between the T300HT fibers and the PyC through the functional groups on the fibers surface. After heat treatment, the fiber stiffness increased but the fibers become more brittle in shear due to their greater orientation anisotropy. A partial failure is induced below the surface of the T300HT fibers, with or without PyC, before mechanical loading, due to the strong interfacial cohesion. This failure below the fibers surface leads to a highly damaged interfacial region driven by the presence of the nanoporosities in the microstructure of these fibers. During mechanical tests, matrix cracks could be deflected in this intermediate weakly organized region between T300HT fibers and PyC (or SiC). Consequently, the T300HT/SiC and T300HT/PyC/SiC composites both exhibit a moderate to high F/M coupling and similar mechanical properties with a fracture strain of 0.5%.

This damage mechanism is not possible for the T300 fibers, which are weakened by the interfacial decohesions induced prior the mechanical test during the composite cool-down. The T300 fibers/PyC interfacial coupling does not prevent the penetration of matrix cracks within the fibers. Indeed, the intensity of the T300/PyC fiber coupling is strong due to the high microstructural organization of the deposited PyC first planes and the chemical compatibility between the T300 fibers and the carbon interphase. The PyC interphase is damaged and partial debonded from the SiC matrix before any external loading. The mechanical load on the T300 fibers is then stronger, which causes the early failure of the fibers. The PyC interphase does not allow improving the failure properties of these composites and does not ensure its function of cracks deflector within these composites. This leads to a very low damage tolerance for T300/PyC/SiC composite similar to that of T300/SiC composite.

5. Conclusion

This study has led to understand the impact of the carbon fibers thermal treatment on the mechanical behavior and on the fiber/matrix coupling of C/SiC composites. When these composites are manufactured with T300 fibers heat-treated at 1600°C (T300HT), the bond strength and the failure mode of the carbon-rich interfaces are optimized.

The improvement of the fiber/matrix coupling of the T300HT/SiC composites was influenced neither by the thermal residual stresses from the C/SiC manufacturing process nor by the increase in fiber stiffness due to heat treatment. The study also revealed the negligible effect of the PyC interphase on the mechanical behavior.

However, we could identify the key role of the surface characteristics on the damage mechanisms of C/SiC composites. The surface reactivity of these fibers, which increases due to heat pretreatment, results in strong interfacial cohesion. After mechanical loading, favored by the nanoporosities and the orientation anisotropy of the structure of the T300HT fiber, the F/M interface becomes a highly damaged region where the matrix cracks are better deflected.

Declaration of interests

The authors declare that they have no known competing financial interests or personal relationships that could have appeared to influence the work reported in this paper.

Acknowledgements

The authors are very grateful to S. Poissonnet for the FIB preparation and scientific discussions, G. Brabant for his help in SEM images and G. Loupias for mechanical tests.

References

[1] S.-J. Park, *Carbon Fibers*, vol. 210, Dordrecht: Springer Netherlands, 2015.

[2] W. Krenkel and F. Berndt, 'C/C–SiC composites for space applications and advanced friction systems', *Mater. Sci. Eng. A*, vol. 412, no. 1, pp. 177–181, Dec. 2005.

[3] B. Heidenreich, 'C/SiC and C/C-SiC Composites', *Ceram. Matrix Compos.*, pp. 147–216, Sep. 2014.

[4] S. Kumar, K. C. Shekar, B. Jana, L. M. Manocha, and N. Eswara Prasad, 'C/C and C/SiC Composites for Aerospace Applications', in *Aerospace Materials and Material Technologies : Volume 1: Aerospace Materials*, N. E. Prasad and R. J. H. Wanhill, Eds. Singapore: Springer Singapore, 2017, pp. 343–369.

[5] Q. Zhang and G. Li, 'A Review of the Application of C/SiC Composite in Thermal Protection System', *Multidiscip. Model. Mater. Struct.*, Feb. 2009.

[6] J. P. Singh *et al.*, *Processing and Properties of Advanced Ceramics and Composites IV*. John Wiley & Sons, 2012.

[7] W. Krenkel, 'Carbon Fibre Reinforced Silicon Carbide Composites (C/SiC, C/C-SiC)', in *Handbook of Ceramic Composites*, N. P. Bansal, Ed. Boston, MA: Springer US, 2005, pp. 117–148.

[8] A. G. Evans, « Mechanical performance of fiber-reinforced ceramic matrix composites », Materials *Science and Engineering, A*, vol. 107, pp. 227-39, 1989.

[9] R. R. Naslain, 'The design of the fibre-matrix interfacial zone in ceramic matrix composites', *Compos. Part Appl. Sci. Manuf.*, vol. 29, no. 9, pp. 1145–1155, Jan. 1998,

[10] E. Inghels and J. Lamon, 'Caractérisation de l'endommagement de composites tissés à matrice SiC', *Rev. Phys. Appliquée*, vol. 23, no. 3, pp. 193–200, Mar. 1988.

[11] J.-L. Bobet and J. Lamon, 'Thermal residual stresses in ceramic matrix composites—I. Axisymmetrical model and finite element analysis', *Acta Metall. Mater.*, vol. 43, no. 6, pp. 2241–2253, Jun. 1995.

[12] C. Sauder, J. Lamon, and R. Pailler, 'The tensile behavior of carbon fibers at high temperatures up to 2400 °C', *Carbon*, vol. 42, no. 4, pp. 715–725, Jan. 2004.

[13] H. Mei, H. Li, Q. Bai, Q. Zhang, and L. Cheng, 'Increasing the strength and toughness of a carbon fiber/silicon carbide composite by heat treatment', *Carbon*, vol. 54, pp. 42–47, Apr. 2013.

[14] H. Xiao, Y. Lu, W. Zhao, and X. Qin, 'The effect of heat treatment temperature and time on the microstructure and mechanical properties of PAN-based carbon fibers', *J. Mater. Sci.*, vol. 49, no. 2, pp. 794–804, Jan. 2014.

[15] H. T. Liu, L. W. Yang, X. Sun, H. F. Cheng, C. Y. Wang, W. G. Mao, and J. M. Molina-Aldareguia, 'Enhancing the fracture resistance of carbon fiber reinforced SiC matrix composites by interface modification through a simple fiber heat-treatment process', *Carbon*, vol. 109, pp. 435–443, Nov. 2016.

[16] C. Cazeneuve, J. E. Castle, and J. F. Watts, 'The structure of the interface in carbon fibre composites by scanning Auger microscopy', *J. Mater. Sci.*, vol. 25, no. 4, pp. 1902–1908, Apr. 1990.

[17] V. Serin, R. Fourmeaux, Y. Kihn, J. Sevely, and M. Guigon, 'Nitrogen distribution in high tensile strength carbon fibres', *Carbon*, vol. 28, no. 4, pp. 573–578, Jan. 1990.

[18] M. Guigon, 'Relation entre la microtexture et les propriétés mécaniques et électriques des fibres de carbone ex-polyacrylo-nitrile', thesis, Compiègne, 1985.

[19] G. Zhou, J. H. Byun, S. B. Lee, J. W. Yi, W. Lee, S. K. Lee, B. S. Kim, J. K. Park, S. G. Lee, and L. He, 'Nano structural analysis on stiffening phenomena of PAN-based carbon fibers during tensile deformation', *Carbon*, vol. 76, pp. 232–239, Sep. 2014.

[20] G. Zhou, Y. Liu, L. He, Q. Guo, and H. Ye, 'Microstructure difference between core and skin of T700 carbon fibers in heat-treated carbon/carbon composites', *Carbon*, vol. 49, no. 9, pp. 2883–2892, Aug. 2011.

[21] C. Fellah, J. Braun, C. Sauder, F. Sirotti, and M.-H. Berger, 'Influence of the carbon interface on the mechanical behavior of SiC/SiC composites', *Compos. Part Appl. Sci. Manuf.*, vol. 133, p. 105867, Jun. 2020.

[22] D. F. Li, H. J. Wang, F. He, and X. K. Wang, « Structure and properties of T300 and T700 carbon fibers », *Carbon*, vol. 45, n° 6, pp. 1379, 2007.

[23] J. D. H. Hughes, 'The carbon fibre/epoxy interface—A review', *Compos. Sci. Technol.*, vol. 41, no. 1, pp. 13–45, Jan. 1991.

[24] Y. Zhou, D. Jiang, and Y. Xia, 'Tensile mechanical behavior of T300 and M40J fiber bundles at different strain rate', *J. Mater. Sci.*, vol. 36, no. 4, pp. 919–922, Feb. 2001.

[25] N. P. Bansal and J. Lamon, *Ceramic Matrix Composites: Materials, Modeling and Technology*. John Wiley & Sons, 2014.

[26] A. D. Haubold, R. B. More, and J. C. Bokros, 'Carbons', in *Handbook of Biomaterial Properties*, J. Black and G. Hastings, Eds. Boston, MA: Springer US, 1998, pp. 464–477.

[27] S. C. Bennett and D. J. Johnson, 'Electron-microscope studies of structural heterogeneity in pan-based carbon fibres', *Carbon*, vol. 17, no. 1, pp. 25–39, Jan. 1979.

[28] M. Guigon, A. Oberlin, and G. Desarmot, 'Microtexture and structure of some high tensile strength, PAN-base carbon fibres', *Fibre Sci. Technol.*, vol. 20, no. 1, pp. 55–72, Jan. 1984.

[29] A. Hasegawa, A. Kohyama, R. H. Jones, L. L. Snead, B. Riccardi, and P. Fenici, 'Critical issues and current status of SiC/SiC composites for fusion', *J. Nucl. Mater.*, vol. 283–287, pp. 128–137, Dec. 2000.

[30] F. Polack, M. Silly, C. Chauvet, B. Lagarde, N. Bergeard, M. Izquierdo, O. Chubar, D. Krizmancic, M. Ribbens, J. P. Duval, and C. Basset, 'TEMPO: a New Insertion Device Beamline at SOLEIL for Time Resolved Photoelectron Spectroscopy Experiments on Solids and Interfaces', *AIP Conf. Proc.*, vol. 1234, no. 1, pp. 185–188, Jun. 2010.

[31] A. Jablonski and C. J. Powell, "NIST Electron Inelastic-Mean-Free-Path Database", *National Institute of Standards and Technology, Gaithersburg*, 2010.

[32] H. Mei, 'Measurement and calculation of thermal residual stress in fiber reinforced ceramic matrix composites', *Compos. Sci. Technol.*, vol. 68, no. 15, pp. 3285–3292, Dec. 2008.

[33] G. Camus, L. Guillaumat, and S. Baste, 'Development of damage in a 2D woven C/SiC composite under mechanical loading: I. Mechanical characterization', *Compos. Sci. Technol.*, vol. 56, no. 12, pp. 1363–1372, Jan. 1996.

[34] J.-L. Bobet, R. Naslain, A. Guette, N. Ji, and J.-L. Lebrun, 'Thermal residual stresses in ceramic matrix composites—II. Experimental results for model materials', *Acta Metall. Mater.*, vol. 43, no. 6, pp. 2255–2268, Jun. 1995.

[35] A. Michaux, C. Sauder, G. Camus, and R. Pailler, 'Young's modulus, thermal expansion coefficient and fracture behavior of selected Si–B–C based carbides in the 20–1200°C temperature range as derived from the behavior of carbon fiber reinforced microcomposites', *J. Eur. Ceram. Soc.*, vol. 27, no. 12, pp. 3551–3560, Jan. 2007.

[36] Z. Hashin, 'Analysis of composite materials—a survey', 1983, pp. 481-505.

[37] Z. Hashin, 'Analysis of Properties of Fiber Composites With Anisotropic Constituents', *J. Appl. Mech.*, vol. 46, no. 3, pp. 543–550, Sep. 1979.

[38] C. Pradere and C. Sauder, 'Transverse and longitudinal coefficient of thermal expansion of carbon fibers at high temperatures (300–2500K)', *Carbon*, vol. 46, no. 14, pp. 1874–1884, Nov. 2008.

[39] E. Buet, C. Sauder, D. Sornin, S. Poissonnet, J.-N. Rouzaud, and C. Vix-Guterl, 'Influence of surface fibre properties and textural organization of a pyrocarbon interphase on the interfacial shear stress of SiC/SiC minicomposites reinforced with Hi-Nicalon S and Tyranno SA3 fibres', *J. Eur. Ceram. Soc.*, vol. 34, no. 2, pp. 179–188, Feb. 2014.

[40] J. Braun, C. Guéneau, T. Alpettaz, C. Sauder, E. Brackx, R. Domenger, S. Gossé, and F. Balbaud-Célérier, 'Chemical compatibility between UO2 fuel and SiC cladding for LWRs. Application to ATF (Accident-Tolerant Fuels)', *J. Nucl. Mater.*, vol. 487, pp. 380–395, Apr. 2017.

[41] Z. Dai, F. Shi, B. Zhang, M. Li, and Z. Zhang, 'Effect of sizing on carbon fiber surface properties and fibers/epoxy interfacial adhesion', *Appl. Surf. Sci.*, vol. 257, no. 15, p. 6980, 2011.

[42] Z. Dai, B. Zhang, F. Shi, M. Li, Z. Zhang, and Y. Gu, 'Effect of heat treatment on carbon fiber surface properties and fibers/epoxy interfacial adhesion', *Appl. Surf. Sci.*, vol. 257, no. 20, p. 8457, 2011.

[43] J. J. Sha, J. X. Dai, J. Li, Z. Q. Wei, J.-M. Hausherr, and W. Krenkel, 'Influence of thermal treatment on thermo-mechanical stability and surface composition of carbon fiber', *Appl. Surf. Sci.*, vol. 274, pp. 89-89–94, Jun. 2013.

[44] M. B. Neĭman, B. M. Kovarskaya, L. I. Golubenkova, A. S. Strizhkova, I. I. Levantovskaya, and M. S. Akutin, 'The thermal degradation of some epoxy resins', *J. Polym. Sci.*, vol. 56, no. 164, pp. 383–389, 1962.

[45] A. Bismarck, R. Tahhan, J. Springer, A. Schulz, T. M. Klapötke, H. Zeil, and W. Michaeli, 'Influence of fluorination on the properties of carbon fibres', *J. Fluor. Chem.*, vol. 84, no. 2, pp. 127–134, Sep. 1997.

[46] T. J. Moravec and T. W. Orent, 'Electron spectroscopy of ion beam and hydrocarbon plasma generated diamondlike carbon films', *J. Vac. Sci. Technol.*, vol. 18, no. 2, pp. 226–228, Mar. 1981.

[47] J. Charlier, V. Detalle, F. Valin, C. Bureau, and G. Lécayon, 'Study of ultrathin polyamide-6,6 films on clean copper and platinum', *J. Vac. Sci. Technol. A*, vol. 15, no. 2, pp. 353–364, Mar. 1997.

[48] S. Delpeux, F. Beguin, R. Benoit, R. Erre, N. Manolova, and I. Rashkov, 'Fullerene core star-like polymers—1. Preparation from fullerenes and monoazidopolyethers', *Eur. Polym. J.*, vol. 34, no. 7, pp. 905–915, Jul. 1998.

[49] R. P. Socha, K. Laajalehto, and P. Nowak, 'Influence of the surface properties of silicon carbide on the process of SiC particles codeposition with nickel', *Colloids Surf. Physicochem. Eng. Asp.*, vol. 208, no. 1, pp. 267–275, Aug. 2002.

[50] C. Vincent, H. Vincent, M. P. Berthet, T. Piquero, and J. Bouix, 'ESCA characterization of boron and silicon carbide mixed layers deposited on HR and HM carbon fibres by RCVD: properties of the as-coated fibres', *Compos. Part Appl. Sci. Manuf.*, vol. 27, no. 5, pp. 365–377, Jan. 1996.

[51] N. M. D. Brown, J. A. Hewitt, and B. J. Meenan, 'X-ray-induced beam damage observed during x-ray photoelectron spectroscopy (XPS) studies of palladium electrode ink materials', *Surf. Interface Anal.*, vol. 18, no. 3, pp. 187–198, Mar. 1992.

[52] T. L. Barr and S. Seal, 'Nature of the use of adventitious carbon as a binding energy standard', *J. Vac. Sci. Technol. A*, vol. 13, no. 3, pp. 1239–1246, May 1995.

[53] N. Dilsiz and J. P. Wightman, 'Surface analysis of unsized and sized carbon fibers', *Carbon*, vol. 37, no. 7, pp. 1105–1114, Jan. 1999.

[54] M. Guzzo, J. J. Kas, L. Sponza, C. Giorgetti, F. Sottile, D. Pierucci, M. G. Silly, F. Sirotti, J. J. Rehr, and L. Reining, 'Multiple satellites in materials with complex plasmon spectra: From graphite to graphene', *Phys. Rev. B*, vol. 89, no. 8, p. 085425, Feb. 2014.

[55] J. Lamon and J. L. Bobet, 'Influence des contraintes résiduelles sur le comportement mécanique des composites à matrice céramique', *Rev. Métallurgie*, vol. 94, no. 2, pp. 207–218, Feb. 1997.

[56] C. Yanjun, J. Guiqiong, W. Bo, and L. Wei, 'Elastic behavior analysis of 3D angle-interlock woven ceramic composites', *Acta Mech. Solida Sin.*, vol. 19, no. 2, pp. 152–159, Jun. 2006.

[57] Y. Xu, L. Cheng, L. Zhang, H. Yin, and X. Yin, 'Mechanical properties of 3D fiber reinforced C/SiC composites', *Mater. Sci. Eng. A*, vol. 300, no. 1, pp. 196–202, Feb. 2001.

[58] F. Lamouroux, X. Bourrat, R. Nasalain, and J. Sevely, 'Structure/oxidation behavior relationship in the carbonaceous constituents of 2D-C/PyC/SiC composites', *Carbon*, vol. 31, no. 8, pp. 1273–1288, Jan. 1993.